Controlling the Neuronal Differentiation of Stem Cells by the Intracellular Delivery of Retinoic Acid-Loaded Nanoparticles

João Maia,[†,∥] Tiago Santos,[‡,∥] Sezin Aday,[§] Fabienne Agasse,[‡] Luísa Cortes,[⊥] João O. Malva,[‡] Liliana Bernardino,[‡,*] and Lino Ferreira[§,*]

[†]Chemical Engineering Department, University of Coimbra, Pinhal de Marrocos, 3030-290 Coimbra, Portugal and [‡]Neuroprotection and Neurogenesis in Brain Repair Group, [§]Biomaterials and Stem Cell-Based Therapeutics Group, and [⊥]Microscopy and Flow Cytometry Unit, Center for Neuroscience and Cell Biology, University of Coimbra, 3004-517 Coimbra, Portugal. [∥]These authors contributed equally to this work.

ABSTRACT The manipulation of endogenous stem cell populations from the subventricular zone (SVZ), a neurogenic niche, creates an opportunity to induce neurogenesis and influence brain regenerative capacities in the adult brain. Herein, we demonstrate the ability of polyelectrolyte nanoparticles to induce neurogenesis exclusively after being internalized by SVZ stem cells. The nanoparticles are not cytotoxic for concentrations equal or below 10 μg/mL. The internalization process is rapid, and nanoparticles escape endosomal fate in a few hours. Retinoic acid-loaded nanoparticles increase the number of neuronal nuclear protein (NeuN)-positive neurons and functional neurons responding to depolarization with KCl and expressing NMDA receptor subunit type 1 (NR1). These nanoparticles offer an opportunity for *in vivo* delivery of proneurogenic factors and neurodegenerative disease treatment.

KEYWORDS: stem cells · nanoparticles · retinoic acid · neuronal differentiation · intracellular trafficking

Several biomolecules have the capacity to differentiate stem cells' progeny toward desired lineage-specific precursors.[1−4] However, the administration of some of these bioactive factors presents a significant challenge because of their poor water solubility, short half-life, and potentially undesired side effects. One example is retinoic acid (RA) which interacts with members of the hormone receptor superfamily, including the RA receptor (RAR) and the retinoid X receptor (RXR), located in the cell nuclei.[5] These receptors heterodimerize and bind to a DNA sequence called retinoic acid-response element (RARE), activating gene transcription involved in cell proliferation, differentiation, and apoptosis. Many factors regulate neurogenesis, and several studies have demonstrated that RA is able to induce the differentiation of progenitor cells into neuronal cells,[5−7] suggesting that this molecule is a good candidate for enhancing postinjury neurogenesis. However, RA is rapidly metabolized by cells and has low solubility in aqueous solutions.[8] In addition, the use of this biomolecule in an *in vivo* setting for the differentiation of resident stem/progenitor cells remains elusive.

Nanoparticles can be an excellent platform to ensure intracellular transport and controlled release of RA.[9−11] Several nanoparticle formulations have been developed for the release of this molecule.[9−11] However, until now, none of the reported formulations was designed to deliver RA within cells and particularly for the differentiation of stem/progenitor cells. Nanoparticles can be internalized *via* endocytosis, macropinocytosis, or phagocytosis, but these processes confine the compounds to closed vesicles (endosomes or phagosomes), where the pH is progressively lowered to 5.5−6.5.[12,13] Polycations, such as polyethylenimine, that absorb protons in response to the acidification of endosomes (*i.e.*, cationic polymers with a p*K* around or slightly below physiological pH) can disrupt these vesicles *via* the "proton sponge" effect that promotes the swelling of the endosome *in situ*.[14,15] Once the polymeric nanoparticles reach the cytosol, the bioactive molecule may be released by desorption, diffusion through the nanoparticle, or nanoparticle erosion.

Herein, we present a novel strategy to differentiate the progeny of stem cells into neurons using nanoparticles able to intracellularly release RA. We demonstrate that the internalization of the RA-loaded nanoparticles has a minimal effect on cell viability and proliferation but a large impact on

*Address correspondence to lino@biocant.pt, libernardino@gmail.com.

Received for review July 21, 2010 and accepted December 07, 2010.

Published online December 20, 2010. 10.1021/nn101724r

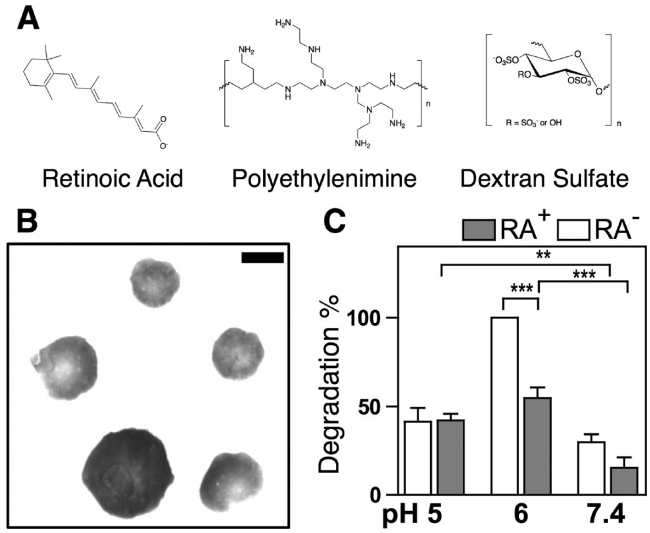

Figure 1. Physico-chemical properties of the nanoparticles. (A) Chemical structures of retinoic acid (RA), polyethylenimine (PEI), and dextran sulfate (DS). (B) Transmission electron microscopy (TEM) images of RA^+-NPs. Scale bar: 200 nm. (C) Mass loss on nanoparticles suspended in buffered solutions at pH 5.0, 6.0, and 7.4 for 7 days at 37 °C. Nanoparticles with or without RA were used in these degradation studies. Results are shown as mean ± SD, $n = 6$. ** and * denote statistical significance $P < 0.01$ and $P < 0.001$, respectively.**

differentiation. Importantly, nanoparticle-conditioned medium is unable to promote the differentiation of stem/progenitor cells, indicating that neuronal differentiation is only mediated by internalization of the nanoparticles.

RESULTS AND DISCUSSION

Nanoparticles were prepared by complex coacervation, that is, through the electrostatic interaction of polyethylenimine (PEI, polycation) and dextran sulfate (DS, polyanion) (Figure 1A). Initially, complexes of RA with PEI were formed by the electrostatic interactions of the carboxyl groups of RA with the amine groups of PEI. Maximum loading is obtained for a ratio of amino groups to carboxylic acid groups of about 2:1.[9] In this work, we used a ratio between 4:1 (for the NP formulation DS/PEI with weight ratio of 5.0) and 17:1 (for the NP formulation DS/PEI with weight ratio of 0.2), only considering the primary amines present in PEI. The electrostatic interaction between RA and PEI is confirmed by a shift in the RA peak from 350 to 300 nm, as confirmed by spectrophotometry (Supporting Information Figure 1). These complexes formed nanoparticles with 100 to 250 nm in diameter, although they tend to stick together and are not easy to resuspend. To stabilize the nanoparticle formulation, DS and zinc sulfate were added in successive steps.[16] The physical cross-linking of DS with PEI has been confirmed previously by Fourier transform infrared (FTIR) analysis.[16] Nanoparticles without zinc sulfate tend to aggregate and form large particles. Mannitol was added to the NP suspension during centrifugation steps and lyophilization to prevent their aggregation.

Three different weight ratios of DS relative to PEI were selected for our initial screening: 5.0 (large excess of DS), 1.0 (similar weight of both polymers), and 0.2 (large excess of PEI). In each formulation, we determined particle size, zeta-potential, and RA loading efficiency. A Brookhaven ZetaPALS analyzer was used to evaluate NP zeta-potential and size distribution (deionized water). The number-weighting profile of all formulations tested was usually unimodal (>99%) (Supporting Information Figure 2). The formulation DS/PEI weight ratio of 5 yielded nanoparticles with an average diameter between 40 and 120 nm and a negative net charge, while the formulation DS/PEI weight ratio of 1 yielded large aggregates of nanoparticles (diameter >500 nm) with a positive net charge (Table 1). This is in line with other results previously reported, indicating that an excess of one of the NP components is needed to act as a colloidal protective agent and preventing the coalescence of the NPs.[16] Nanoparticles prepared from the formulation DS/PEI weight ratio of 0.2 had an average diameter between 80 and 90 nm; however, presenting a significantly higher RA loading efficiency (48 *versus* 2%) and positive net charge (15 *versus* 2 mV) than the other formulations tested. The high loading efficiency is explained by the high content of PEI able to interact with RA. On the basis of the loading capacity and net charge results, nanoparticles obtained from the formulation 0.2 were selected for subsequent experiments. The morphology of these nanoparticles was then characterized by transmission electron microscopy (TEM). TEM micrographs (Figure 1B) show a similar range of sizes as observed by DLS.

TABLE 1. Physico-Chemical Characteristics of DS/PEI Nanoparticles Either with or without RA

formulation	ratio[a] w/w	charge ratio[b]	η[c] %	ζ[d] mV	emulsion[e] nm	RV[f]	NP[g] Nm	RV[f]	LE[h] %	RA payload[i] μg/mg
DS/PEI	5	7.1	1	−34.7 ± 3.0	43.4	0.074	74	0.311		
DS/PEI + RA	5	7.4	6.2	−42.6 ± 8.1	115	0.283	67	0.557	2.2 ± 1.2	18.6 ± 9.2
DS/PEI	1	1.4	n.a.	n.a.	541[j]	0.510[j]	n.a.	n.a.		
DS/PEI + RA	1	1.5	7.3	+1.9 ± 0.5	711[j]	0.228[j]	n.a.	n.a.	0.4 ± 0.2	2.5 ± 1.5
DS/PEI	0.2	0.3	22.5	+14.9 ± 2.8	91	0.044	61	0.078		
DS/PEI + RA	0.2	0.4	34.12	+15.6 ± 1.4	80	0.074	224	0.503	48.3 ± 15.9	86.1 ± 28.4

[a]Polyelectrolyte initial weight ratio. The experimental ratio for the 0.2 and 0.2RA formulations was 0.585 and 0.599, respectively. [b]Charge ratio (±). [c]Yield (without mannitol). [d]Zeta-potential in mV. [e]Peak diameter after the emulsion. [f]Relative variance. [g]Nanoparticle size after freeze-drying and resuspended in aqueous buffer. [h]Loading efficiency. [i]Amount of RA per mass of nanoparticle (without mannitol). [j]Formation of aggregates; values after removing the formed agglomerates.

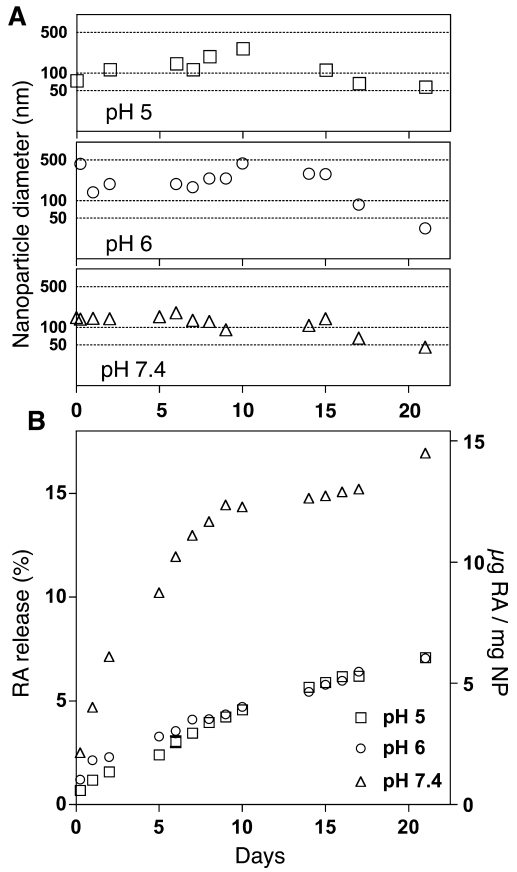

Figure 2. Diameter and release profile of RA$^+$-NPs. Diameter variation (A) and release profile (B) of RA$^+$-NPs suspended in buffered solutions at pH 5.0, 6.0, and 7.4 over 21 days at 37 °C.

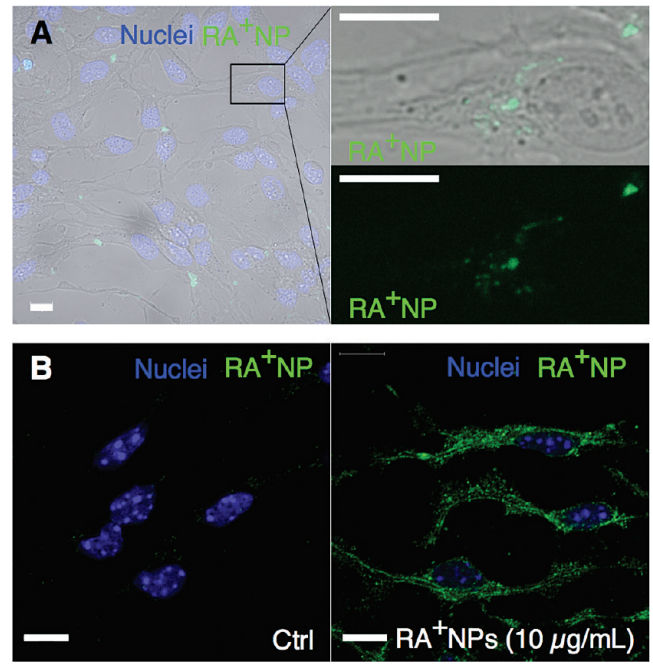

Figure 3. Cellular nanoparticle uptake. (A) Confocal live imaging of SVZ cells after exposure for 5 h to FITC-labeled RA$^+$-NPs (50 μg/mL). Hoechst-33342 staining (blue) was used to visualize cell nuclei. Crop images show both transmission and FITC channel or FITC channel alone. (B) Confocal microscopy photomicrographs of untreated or FITC-labeled RA$^+$-NP-treated (10 μg/mL) SVZ cells for 18 h, imunostained with anti-FITC antibody and Hoechst-33342. Scale bars are 10 μm.

The dissolution profile of nanoparticles is affected by pH. The dissolution of the nanoparticles (~10 mg/mL) was evaluated at pH 7.4, 6.0, and 5.0 under agitation at 37 °C. This pH range is typically found at the cytoplasm and intracellular organelles.[13] After 7 days, the suspensions were centrifuged, lyophilized, and finally weighed. Interestingly, the disassembly of RA-containing nanoparticles (RA$^+$-NPs) at pH 6.0 and 7.4 was lower than blank nanoparticles (RA$^-$-NPs) (Figure 1C). This might reflect differences in the cross-linking of both preparations. RA might act as a cross-linker agent, where the carboxyl group interacts electrostatically with the amine groups of PEI, and the aromatic group interacts hydrophobically with the aromatic group of another RA molecule. RA$^+$-NPs showed a mass loss of 15.4 ± 5.9, 42 ± 3.8, and 54.5 ± 6.3% at pH 7.4, 5.0, and 6.0, respectively, over 7 days (Figure 1C). Our results indicate that acidic pH enhanced the degradation of the nanoparticles likely due to the protonation of PEI amine groups (in excess relative to the sulfate groups in DS) and the concomitant repulsion between positive charges.[17]

The release of RA from nanoparticles is dependent on the external pH. Polyelectrolyte complexes change their three-dimensional conformation according to the pH, affecting the release of RA. To evaluate this effect, nanoparticles were incubated at pH 7.4, 6.0, or 5.0 at 37 °C under agitation. At determined times, the nanoparticle suspensions were centrifuged and the supernatant was evaluated by spectrophotometry at 350 nm. The nanoparticle diameter was also evaluated at each time point (Figure 2A). At pH 7.4, the initial diameter (~100 nm) is roughly maintained over 15 days, decreasing afterward to approximately 60 nm. At pH 6.0 and 5.0, higher aggregation was observed for all of the time points; however, the population with diameters between 100 and 1000 nm (number-weighting average) accounted for most (>95%) of the nanoparticles in suspension (Figure 2A).

Taking into account that RA solubility is approximately 63 ng *per* mL at physiological pH,[8] most of the RA released at pH 7.4 is complexed with PEI (Figure 2B). Indeed, the complexation of RA to PEI is confirmed by a shift in the RA peak at 350 nm, which is not affected by the subsequent addition of DS (Supporting Information Figure 1). Interestingly, the release of RA at pH 5.0 or 6.0 is much lower than pH 7.4 over the same period of time. This can be due to the crystallization of the RA and the aggregation of the nanoparticles at acidic pH values, which decreases RA diffusion from the nanoparticles.[18,19] Alternatively, RA is released by the nanoparticles at higher percentages than the values assessed, and the low values observed by us is because

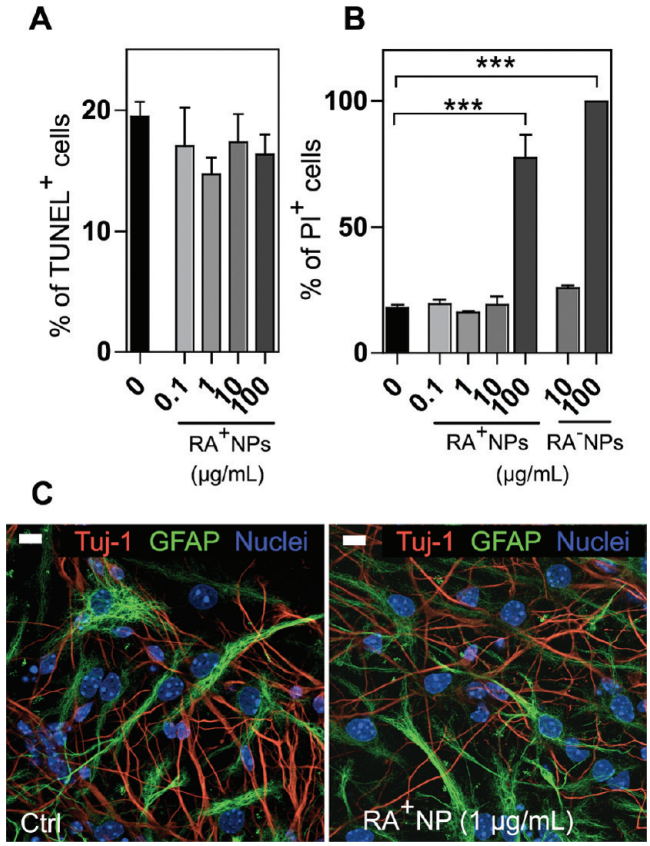

Figure 4. Cell viability after RA$^{\pm}$-NPs uptake. (A) Percentage of TUNEL-positive cells in control cultures and in cultures exposed to RA^{+}-NPs for 2 days. Data are expressed as mean ± SEM (n = 4−8 coverslips). (B) Percentage of PI-positive cells in control cultures and in cultures exposed to RA^{+}-NPs or RA^{-}-NPs for 2 days. Data are expressed as mean ± SEM (n = 4−9 coverslips). ***$P < 0.001$ using Dunnett's multiple comparison test. (C) Representative confocal microscopy photomicrographs showing a typical morphology of Tuj1-positive neurons (red), GFAP-positive glia (green), and Hoechst-33342 staining (blue nuclei) in SVZ cells maintained for 7 days in the absence (control) or in the presence of RA^{+}-NPs (1 μg/mL). Scale bars are 10 μm.

RA precipitates at acidic pH, circumventing its real quantification.

RA^{+}-NPs could potentially be used to induce neurogenesis and influence the brain regenerative capacities. In adult mammalian brain, neurogenesis persists in restricted neurogenic niches. These resources play a central role in the generation and integration of new neurons into pre-existing neural circuitry and are crucial for the maintenance of brain integrity and plasticity.[20−22] The SVZ is the main neurogenic niche of the adult rodent brain[20−22] and contains a population of neural stem cells that can give rise to neurons, astrocytes, and oligodendrocytes. Therefore, SVZ cells have a huge potential for stem-cell-based brain repair strategies. Previous studies have shown that nanoparticles (typically below 100 nm) formed by PEI (polycation) complexed with DNA (polyanion) can be internalized by adult mammalian brain cells.[23−25] However, in spite of the importance of SVZ neural stem cells for brain physiology and repair, there is no consistent information concerning nanoparticle uptake and intracellular drug release in SVZ cells.

To evaluate the kinetics of nanoparticle uptake by SVZ cells, they were exposed to fluorescein isothiocyanate (FITC)-conjugated nanoparticles, and their uptake was assessed by confocal live cell imaging (video in the Supporting Information) and immunocytochemistry. RA^{+}NPs suspended in cell medium showed a diameter of 250 nm and a zeta-potential of −22.4 ± 4.4 mV. The negative zeta-potential indicates a rapid electrostatic interaction with proteins and other elements from the culture medium. One hour after cell treatment, nanoparticles accumulate rapidly in cell cytoplasm (data not shown). This accumulation becomes even more expressive at 5 h (Figure 3A). This is in line with other studies, showing that PEI-based nanoparticles can rapidly escape endosomal fate due to their buffering capacity, leading to osmotic swelling and rupture of endosomes.[15] At 18 h after cell treatment, the FITC-conjugated nanoparticles are distributed over all of the cell cytoplasm (Figure 3B).

To determine the cytotoxicity of these nanoparticles, SVZ neurospheres were exposed to RA^{+}-NPs or RA^{-}-NPs for 2 days and cell death, presumably involving apoptosis or necrosis, was then evaluated by terminal deoxynucleotidyl transferase-mediated dUTP nick end labeling (TUNEL) and propidium iodide (PI) staining, respectively. No significant effect on cell apoptosis was observed for all the experimental groups tested with nanoparticle concentrations up to 100 μg/mL (Figure 4A). In contrast, cell necrosis increases significantly for nanoparticle concentrations of 100 μg/mL (~4-fold) (77.3 ± 9.1%; n = 4 coverslips; 2938 cells counted; $P < 0.0001$), relative to the control (17.8 ± 1.3%; n = 9 coverslips; 8618 cells counted) (Figure 4B). The toxic effects of 100 μg/mL RA^{+}-NPs was not due to RA since the void formulation RA^{-}-NPs was equally toxic at the same concentration (Figure 4B). On the basis of these results, RA^{+}-NPs are not cytotoxic for concentrations equal or below 10 μg/mL. Moreover, at these concentrations, the internalization of the nanoparticles did not affect significantly the morphology of the cells. Untreated cells or cells treated with RA^{+}-NPs (1 μg/mL) for 7 days were characterized by immunocytochemistry against neuron-specific class III β-tubulin (Tuj1) and glial fibrillary acidic protein (GFAP). RA^{+}-NP-treated cells present a healthy morphology undistinguishable from untreated cells (Figure 4C).

To investigate the effect of RA^{+}-NPs on cell proliferation, SVZ neurospheres were exposed to a wide range of nanoparticle concentrations (0.001 to 10 μg/mL) for 2 days and then exposed to bromodeoxyuridine (BrdU) in the last 4 h of the treatment. BrdU is a synthetic nucleoside that can be incorporated into newly synthesized DNA substituting for thymidine during cell replication. SVZ cells either when grown under proliferative (in serum-free medium with growth factors as free float-

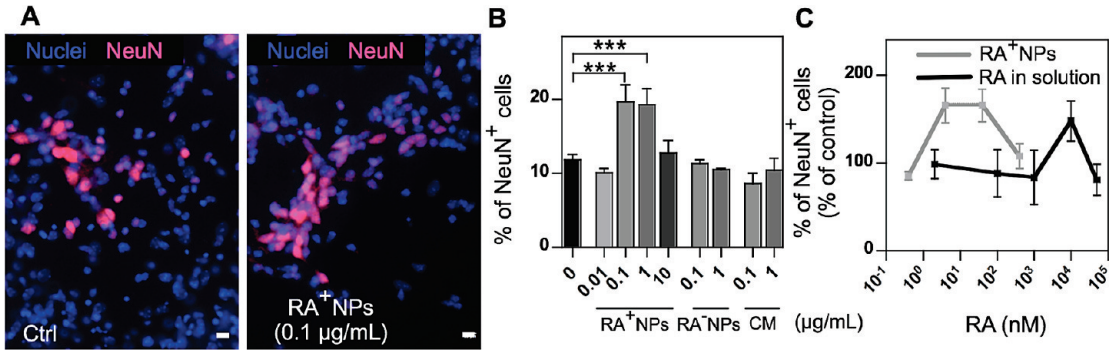

Figure 5. RA$^+$-NPs have a proneurogenic effect. (A) Representative fluorescence photomicrographs of NeuN immunostaining (red) in control cultures and cultures exposed to RA$^+$-NPs (0.1 μg/mL) for 7 days. Hoechst-33342 was used for nuclear staining (blue). (B) Percentage of NeuN-immunostained neurons in SVZ cultures after being exposed for 7 days to RA$^+$-NPs, RA$^-$-NPs, or conditioned medium (CM) obtained from the centrifugation of a nanoparticle suspension left in culture for 7 days. Data are expressed as mean ± SEM (n = 5−15 coverslips). ***$P < 0.001$ using unpaired Student's t test for comparison with SVZ control cultures. (C) Percentage of NeuN-immunostained neurons in SVZ cultures after being exposed for 7 days to RA$^+$-NPs or free-RA (solubilized in DMSO and added to the culture medium at different concentrations). Data are expressed as mean ± SEM (n = 6−15 coverslips).

ing neurospheres) or differentiation (after adherence on poly-D-lysine and in the absence of growth factors) conditions exposed to RA$^+$-NPs had similar proliferation rates as control cells not exposed to nanoparticles (Supporting Information Figure 3).

SVZ cell cultures are mixed cultures of immature cells, neurons, astrocytes, oligodendrocytes, neuronal and glial progenitors in different stages of differentiation.[26−28] In untreated SVZ cultures, we detected about 5−15% of new neurons (detected by SCCI and NeuN immunocytochemistry; Figure 5), which is in accordance with the percentage of neurons obtained from standard methods of isolating neural stem cells *in vitro*.[28,29] To evaluate the effect of RA$^+$-NPs on neuronal differentiation of SVZ cells, the cells were cultured in differentiation conditions for 7 days in media containing the nanoparticles (Supporting Information Figure 4) and then immunolabeled for NeuN, a neuronal-specific nuclear protein present on mature neurons.[30−32] In the presence of RA$^+$-NPs at concentrations of 0.1 μg/mL (19.6 ± 2.3%; n = 5 coverslips; 3460 cells counted; $P < 0.001$) and 1 μg/mL (19.2 ± 2.2%; n = 7 coverslips; 4954 cells counted; $P < 0.001$), a significant increase in the percentage of NeuN-positive cells was observed relative to the untreated cells (11.8 ± 0.6%; n = 13 coverslips; 7306 cells counted) (Figure 5A). The proneurogenic effect mediated by RA$^+$-NPs was absent in cell cultures treated with void nanoparticles (RA$^-$-NPs), suggesting that this effect was due to the RA and not due to the nanoparticle formulation *per se* (Figure 5B). Importantly, the neuronal differentiation effect was absent for high concentrations (>1 μg/mL) of nanoparticles, indicating that an optimal concentration window of RA exists to drive the neuronal commitment of SVZ cells. Most *in vitro* studies, using embryonic stem cells and neural stem cell cultures isolated from the SVZ and hippocampus, suggest that RA exposure stimulates neurogenesis and neuronal maturation.[7,33−37] However, the range of RA concentrations used in these studies was from 0.1 to 1 μM. These concentrations are 100- to 1000-fold higher than the payload of RA from nanoparticles that induces neurogenesis in our studies. Considering the RA payload per milligram of NPs, we found that concentrations of RA payload below 4 nM RA (corresponding to 0.1 μg/mL nanoparticles) and above 40 nM RA (corresponding to 1 μg/mL nanoparticles) did not promote neuronal differentiation (Figure 5C). This is consistent with the effect of RA in animal studies.[38,39] The acute administration of RA (0.15 mg/kg) helped to reverse an age-related deficit in long-term potentiation amplitude and improved the ability of the mice to perform relational learning tasks.[38] In contrast, the long-term systemic administration (1 mg/kg, for 42 days) of RA in mice led to a decrease in both proliferation and neuronal production in the hippocampus, which were accompanied by a significant reduction in the ability to perform a learning task.[39] In this case, one of the RA effects was to suppress SVZ neurogenesis.[39]

Because the differentiation process could be due to RA release either in the medium or within the cell, nanoparticles were left in serum-free media (SFM) devoid of growth factors for 7 days at 37 °C, then centrifuged and the resultant supernatant was collected and used to treat SVZ neurospheres (7 days treatment protocol). Interestingly, no significant proneurogenic effect was observed when the nanoparticle conditioned medium (CM) was added to SVZ cells (Figure 5B). This shows that the differentiation of SVZ cells was only mediated by the internalization of the RA$^+$-NPs and concomitant intracellular release of RA. We speculate that the spatial gradient of RA within the cell is likely the cause of this biological response; however, future studies are needed to completely address this issue.

We also found that free RA solubilized in medium, applying the same treatment protocol as for the NP,

has only achieved a proneurogenic effect with a concentration of 10 μM (1000-fold higher concentration than RA released from nanoparticles; 148.6 ± 22.9% percentage relative to control; $n = 6$ coverslips from 3 independent cell cultures) (Figure 5C). Similarly to what was observed with RA$^+$-NPs, this neuronal differentiation effect was also absent for higher concentrations of free RA (50 μM) (81.3 ± 17.8% percentage relative to control; $n = 6$ coverslips from 3 independent cell cultures). Therefore, RA signaling really depends on an optimal concentration window to drive the neuronal commitment. Importantly, results also stress that neuronal differentiation induced by RA$^+$-NPs requires lower RA concentrations as compared with free RA. Therefore, our formulation is advantageous as comparing to the direct incubation with RA.

To assess functional neuronal differentiation, we measured intracellular calcium ($[Ca^{2+}]_i$) variations in single SVZ cells, following KCl depolarization and histamine stimulation[29] (Supporting Information Figure 4). KCl depolarization leads to the massive entry of Ca^{2+} through voltage-dependent calcium channels in differentiated neurons and is used as a functional marker of neuronal differentiation.[40] Histamine stimulation increases $[Ca^{2+}]_i$ in SVZ immature cells but not in neurons or in glial cells.[29] Therefore, mature neurons have low Hist/KCl ratios (below 0.8).[29] To evaluate $[Ca^{2+}]_i$ variations, SVZ cells were loaded with the Fura-2AM calcium probe, perfused continuously for 15 min with Krebs solution, and subsequently stimulated for 2 min with 50 mM KCl followed by 2 min stimulation with 100 mM histamine (Figure 6A). In control cultures, most of the cells showed a predominant immature-like profile, characterized by an increase in $[Ca^{2+}]_i$ in response to histamine but a negligible response to KCl depolarization. In contrast, SVZ cells treated with RA$^+$-NPs at concentration of 0.1 μg/mL displayed an increase in the $[Ca^{2+}]_i$ in response to KCl but not to histamine stimulation, indicating their neuronal-like state (Ctrl: 4.8 ± 1.9%, 9 coverslips, 838 cells; 0.1 μg/mL: 28.2 ± 5.2%, 8 coverslips, 1117 cells; $P < 0.001$) (Figure 6A). Moreover, these cells were characterized for the expression of NMDA subunit type 1 (NR1) by Western blot analysis. Functional NMDA receptors form the molecular basis of synaptic plasticity and depend on the presence of the channel-forming NR1 subunit.[41] In line with the previous results, SVZ cultures that presented a neuronal-like profile (treated with 0.1 μg/mL of RA$^+$-NPs) also show a higher expression of NR1 (~150% compared to control cultures) (Figure 6B).

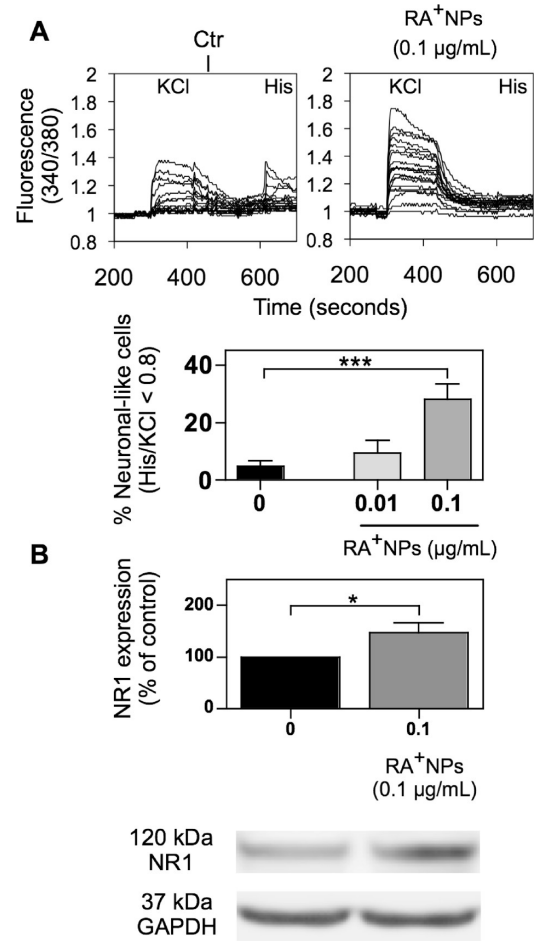

Figure 6. RA$^+$-NPs induce differentiation of SVZ cells into functional neurons. (A) Representative SCCI response profiles of 20 cells in a control culture and in a culture treated with RA$^+$-NPs (0.1 μg/mL). Graph shows percentages of neuronal-like responding cells (Hist/KCl below 0.8) in SVZ control cultures and in cultures exposed to RA$^+$-NPs (0.01 or 0.1 μg/mL) for 7 days. Data are expressed as mean ± SEM ($n = 6-9$ coverslips). ***$P < 0.001$ using Dunnett's multiple comparison test. (B) Graph depicts the percentages relative to control of NR1 protein expression normalized to GAPDH in cultures exposed to RA$^+$-NPs (0.1 μg/mL) for 7 days. Below the graph, a representative Western blot for 120 kDa NR1 and 37 kDa GAPDH expression is shown. The data are expressed as percentage of control ± SEM ($n = 5$). *$P < 0.05$ using paired Student's t test for comparison with SVZ control cultures. Scale bars are 10 μm.

CONCLUSIONS

We report a novel method to modulate the differentiation of SVZ cells into neurons involving the use of RA$^+$-NPs. We show that our NP formulation is very effective in loading RA (86 ± 28 μg of RA per mg of NP), a small molecule with low aqueous solubility, and to release RA at concentrations higher than its solubility limit (>63 ng/mL, at physiological pH[8]) due to its complexation with PEI. We further show that the RA$^+$-NPs have approximately 200 nm diameter, positive net charge, and disassemble preferentially at acidic pH values. These RA$^+$-NPs can be taken up rapidly by SVZ cells (first 5 h) under the tested conditions and localize in the overall cell cytoplasm after 18 h. The NPs are not cytotoxic and do not interfere with cell morphology and proliferation for concentrations below 100 μg/mL. Importantly, our results show that the intracellular internalization of RA$^+$-NPs contributes to neurogenesis and therefore highlights the importance of drug spatial po-

sitioning and concentration in terms of stem cell differentiation. We anticipate that these nanoparticles might be delivered into the brain *via* the nasal cavity, as recently demonstrated for the delivery of cells.[42] Thus, nanoparticle-mediated delivery of neurogenic-inductive factors (proteins, DNA, siRNA, mRNA)[43] might provide a new opportunity for the treatment of various neurodegenerative disorders.

MATERIALS AND METHODS

Materials. *All-trans* retinoic acid, polyethylenimine (PEI, average $M_w \sim 25$ kDa by LS, average $M_n \sim 10$ kDa by GPC, branched), zinc sulfate heptahydrate ($ZnSO_4 \cdot 7H_2O$), ninhydrin reagent solution, Azure A, fluorescein isothiocyanate (FITC), and tungstic acid were purchased from Sigma-Aldrich. Dextran sulfate (DS, $M_w = 500$ kDa) was purchased from Fluka. Dimethyl sulfoxide (DMSO) and ethanol (EtOH) were acquired from Merck. All reagents were used without further purification.

Fluorescent Labeling of PEI. PEI (10 g) was dissolved in 90 mL of borate buffer (pH 8.5), and a 10-fold molar excess of FITC, dissolved in 2 mL of dimethylformamide, was added dropwise and stirred for 1 h. The solution was transferred to a dialysis membrane with 6−8 kDa cutoff and dialyzed against Milli-Q water. The dialyzed solution was freeze-dried for 2−3 days, protected from light.

Preparation of Nanoparticles. Nanoparticles with a weight ratio of DS to PEI of 1 were prepared by adding dropwise 0.6 mL of RA (2% w/v, in DMSO) into 12 mL of PEI (1% w/v, in pH 8.0 borate buffer). The formation of complexes between RA−PEI occurred immediately and was allowed to proceed for 30 min with intense magnetic stirring. Then, 12 mL of DS solution (1% w/v) was added dropwise and stirred for another 5 min. Finally, 1.2 mL of $ZnSO_4$ aqueous solution (1 M) was added and stirred for 30 min. Nanoparticles were centrifuged three times in 5% mannitol solution at 14 000*g* for 20 min. Supernatants from each step were collected to determine PEI and DS amounts in nanoparticles. Resulting nanoparticles were frozen and lyophilized for 4 days to obtain a dry powder. Lyophilized nanoparticles were stored at 4 °C. Similar protocol was adopted for the preparation of nanoparticles with a weight ratio of PEI to DS of 5 and 0.2, by changing the concentration of the polymers accordingly. Blank nanoparticles were prepared using the same procedure in the absence of RA.

Characterization of the Nanoparticles. The morphology of the nanoparticles was evaluated by transmission electron microscopy (Hitachi SU-70, with a STEM detector at 30 kV) following negative staining with tungstic acid solution (1%, w/v; pH 7.5). Initially, an aliquot of lyophilized NPs (5 mg) was resuspended in PBS (1 mL), centrifuged for 5 min at 14 000*g*, resuspended in PBS, centrifuged again, and finally resuspended in PBS (0.5 mg/mL). Five microliters of both sample and tungstic acid solution (1%, w/v; pH 7.5) was placed on a 300 mesh copper grid with a carbon-coated Formvar membrane and dried overnight before examination by TEM.

Particle size was determined using light scattering *via* Zeta PALS zeta-potential analyzer and ZetaPlus particle sizing software, v. 2.27 (Brookhaven Instruments Corporation). Nanoparticles suspended in water and sonicated for short times (<10 min) were used. Typically, all sizing measurements were performed at 25 °C, and all data were recorded at 90°, with an equilibration time of 5 min and individual run times of 60 s (5 runs per measurement). The average diameters described in this work are number-weighted average diameters. The zeta-potential of nanoparticles was determined in a 1 mM KCl pH 6 solution at 25 °C. All data were recorded with at least six runs with a relative residual value (measure of data fit quality) of 0.03.

Determination of Weight Ratio of Cationic to Anionic Polymer in Nanoparticles (Azure A and Ninhydrin Tests). Anionic-to-cationic polymer (DS/PEI) mass ratios in nanoparticles can be determined by subtracting the known amount of PEI and DS in the supernatant of completely centrifuged particles from the initial amount present.[16] The amount of PEI was determined using the ninhydrin assay. For that purpose, the supernatant (20 μL) from the centrifuged nanoparticle suspension was mixed with an acetic acid solution (380 μL; 0.05% w/v) and finally with the ninhydrin reagent (1 mL). The mixture was placed into a boiling water bath for 10 min, cooled to room temperature, and ethanol finally added (3 mL). The amount of PEI was then determined spectrophotometrically at 575 nm using a calibration curve from 10 to 30 μg/mL of PEI.

The amount of unreacted DS in the supernatant was detected spectrophotometrically at 630 nm using an azure A dye binding method in which 400 μL of supernatant from a centrifuged nanoparticle suspension was mixed with 1.0 mL of azure A (10 mg/mL). Again, a calibration curve of 1.0 to 3.5 μg/mL of DS was used to determine the concentration of unknown samples.

Loading Efficiency of RA in Nanoparticles. A given amount of nanoparticle powder was dissolved in 1 mL of DMSO/HCl (9:1) solution and measured the RA absorption at 350 nm. The RA concentration was obtained from a calibration curve from 0.47−0.0023 μg/mL of RA in DMSO/HCl (9:1) solution.

Loading efficiency was calculated using the following equation:

$$\text{loading efficiency} = \frac{\text{amount of RA in the nanoparticles}}{\text{initial amount of RA}} \times 100$$

RA Release from Nanoparticles. Nanoparticles (2.5 mg) were placed in PBS (0.5 mL) and incubated under mild agitation at 37 °C. At specific intervals of time, the nanoparticle suspension was centrifuged (at 20 000 rpm for 20 min) and 0.4 mL of the release medium removed and replaced by a new one. The reserved supernatant was stored at 5 °C until the RA content in release samples was assessed by spectrophotometry at 350 nm. Concentrations of RA were determined by comparison to a standard curve. All analyses were conducted in triplicate.

***In Vitro* Degradation of Polymeric Nanoparticles.** Nanoparticles with or without RA were suspended at ~10 mg/mL in 10 mM PBS (pH 7.4) or 0.2 M citrate buffer pH 5 or 6 and incubated at 37 °C under mild agitation. In one experimental set, the incubation lasted 7 days, after which the nanoparticle suspension was centrifuged (20 000*g* for 15 min) and the pellets were lyophilized for final mass. On the second experimental set, the incubation lasted for 21 days, and at daily intervals, the nanoparticle suspension was centrifuged (20 000*g* for 15 min) and 0.4 mL of the release medium was removed and replaced by a new one for RA quantification and particles size measurements. At the final day, the resulting nanoparticle suspensions were lyophilized for 3 days to obtain a dry powder for mass determination.

SVZ Cell Cultures and Experimental Treatments. All experiments were performed in accordance with NIH and European (86/609/EEC) guidelines for the care and use of laboratory animals. SVZ cells were prepared from 1−3 day old C57BL/6 donor mice as described by Agasse *et al.*[44] Briefly, mice were killed by decapitation, and the brains were removed and placed in calcium- and magnesium-free HBSS solution supplemented with 100 U/mL penicillin and 100 μg/mL streptomycin (Invitrogen, Carlsbad, CA) under sterile conditions. Fragments of SVZ were dissected out of 450 μm thick coronal brain sections using a McIlwain tissue chopper, and then SVZ was digested in 0.025% trypsin (Invitrogen) and 0.265 mM EDTA (Invitrogen) (10 min, 37 °C), following mechanical dissociation with a P1000 pipet. The cell suspension was diluted in SFM composed of Dulbecco's modified eagle medium [(DMEM)/F12 + GlutaMAXTM-I)] supplemented with 100 U/mL penicillin, 100 μg/mL streptomycin, 1% B27 supplement, 10 ng/mL epidermal growth factor (EGF) and 5 ng/mL basic fibroblast growth factor (FGF) 2 (all from Invitrogen). Single cells were then plated on uncoated Petri dishes at a density of 3000 cells/cm^2 and were allowed to develop in an incubator with 5% CO_2 and 95% atmospheric air at 37 °C.

Six day old neurospheres were adhered for 48 h onto 24-well plate poly-D-lysine (0.1 mg/mL)-coated glass coverslips for all experiments except Western blots, which were left adherent onto poly-D-lysine (0.1 mg/mL)-coated 6-well plates, all in SFM devoid of growth factors. Then, the neurospheres were allowed to develop for 2 or 7 days at 37 °C in the presence of a broad range of RA^+-NP concentrations. Cell death assays were done after 2 days of incubation. At the end of the seventh day of treatment, single cell calcium imaging (SCCI) experiments, Western blots, and immunocytochemistry were performed (Supporting Information Figure 4).

To determine whether the proneurogenic effect of RA was due to its release in the cell medium or the nanoparticles internalized, RA^+-NPs were dissolved in SFM devoid of grow factors and incubated for 7 days at 37 °C. Thereafter, the resulting cell medium containing the RA^+-NPs was centrifuged (14 000 rpm, 15 min), nanoparticles were discarded, and the supernatant was recovered and used for conditioned medium (CM) on SVZ cells for 7 days, followed by NeuN immunocytochemistry.

Free *all-trans* RA (Sigma) was solubilized in DMSO and added to the culture medium (DMSO was not toxic when diluted 10.000 times from our stock solution). SVZ cells were incubated for 7 days followed by NeuN immunocytochemistry.

Single Cell Calcium Imaging. To functionally characterize neuronal differentiation in SVZ cells, variations of intracellular calcium concentrations ($[Ca^{2+}]_i$) following stimulation with 50 mM KCl and 100 μM histamine (Sigma-Aldrich) were analyzed. KCl depolarization causes the increase of $[Ca^{2+}]_i$ in neurons, whereas stimulation with histamine increases $[Ca^{2+}]_i$ in stem/progenitor cells.[29] SVZ cultures were loaded for 40 min at 37 °C with 5 μM Fura-2 AM (Invitrogen), 0.1% fatty acid-free bovine serum albumin (BSA), and 0.02% pluronic acid F-127 in Krebs buffer (132 mM NaCl, 1 mM KCl, 1 mM $MgCl_2$, 2.5 mM $CaCl_2$, 10 mM glucose, 10 mM HEPES, pH 7.4). After a 10 min postloading period at room temperature (RT), the coverslip was mounted on RC-25 chamber in a PH3 platform (Warner Instruments, Hamden, CT) on the stage of an inverted Axiovert 200 fluorescence microscope (Carl Zeiss, Göttingen, Germany). Cells (approximately 100 cells per field) were continuously perfused with Krebs and stimulated by applying 100 μM histamine or high-potassium Krebs solution (containing 50 mM KCl, isosmotic substitution with NaCl) by the mean of a fast pressurized (95% air, 5% CO_2 atmosphere) system (AutoMate Scientific Inc., Berkeley, CA). $[Ca^{2+}]_i$ was evaluated by quantifying the ratio of the fluorescence emitted at 510 nm following alternate excitation (750 ms) at 340 and 380 nm, using a Lambda DG4 apparatus (Sutter Instrument, Novato, CA) and a 510 nm long-pass filter (Carl Zeiss) before fluorescence acquisition with a 40× objective and a CoolSNAP digital camera (Roper Scientific, Tucson, AZ). Acquired values were processed using the MetaFluor software (Universal Imaging, Downingtown, PA). KCl and histamine peaks given by the normalized ratios of fluorescence at 340/380 nm were used to calculate the Fura-2 ratios of response to histamine/KCl. The percentage of cells displaying a neuronal-like profile was calculated on the basis of the histamine (Hist)/KCl ratio.

Internalization Studies. In order to visualize the cellular uptake of RA^+-NP by SVZ cells, we performed a live imaging experiment on a confocal microscope (LSM 510 Meta, Carl Zeiss): 50 μg/mL RA^+-NPs were administrated to SVZ neurospheres seeded on glass-bottomed Petri dishes (35 mm, IBIDI, Germany) and incubated at 37 °C for 60 min. For imaging, cells were then placed into a special stage (Heating Insert P Lab-Tek and Incubator S, Pecon) at 37 °C, 5% CO_2 on a confocal laser scanning microscopy (LSM 510 META, Carl Zeiss). This system maintained normal cell culture and allowed multiple regions of interest to be imaged regularly throughout the duration of the experiment. Internalization of NP was followed over a 4 h period (4 frames^{-1}) by detection of FITC bound to the NPs using a 488 nm argon laser (45 mW) for excitation and a 510−550 nm band-pass emission filter and a 63× objective (Plan-ApoChromat, NA 1.4). Differential interference contrast (DIC) images were simultaneously acquired in order to visualize alterations on cell morphology during the experiment. Finally, Hoechst-33342 (2 μg/mL) (Invitrogen) was added in order to visualize nuclei morphology. Images were acquired using a 405 nm diode laser (30 mW) and a band-pass emission filter (420−450 nm).

Western Blots. SVZ cells, previously incubated with RA^+-NPs for 7 days in differentiation conditions, were washed with 0.15 M phosphate-buffered saline (PBS) and incubated in a lysis buffer [0.15 M NaCl, 0.05 M Tris-base, 5 mM EGTA, 1% Triton X-100, 0.5% DOC, 0.1% SDS, 10 mM DTT containing a cocktail of proteinase inhibitors (Roche)]. Total protein concentration from the lysates was determined by BCA assay, and samples were treated with SDS−PAGE buffer [6× concentrated: 350 mM Tris, 10% (w/v) SDS, 30% (v/v) glycerol, 0.6 M DTT, 0.06% (w/v) bromophenol blue], boiled for 5 min at 95 °C, and stored at −20 °C until used for Western blotting. Then, proteins (40 μg of total protein) were resolved in 15% SDS polyacrylamide gels and then transferred to PVDF membranes with 0.45 μm pore size in the following conditions: 300 mA, 90 min at 4 °C in a solution containing 10 mM CAPS and 20% methanol, pH 11 (protocol adapted from Pinheiro *et al.*).[45] Membranes were blocked in Tris buffer saline containing 5% low-fat milk and 0.1% Tween 20 (Sigma) for 1 h at RT and then incubated overnight at 4 °C with the primary antibody rabbit monoclonal anti-NR1 (1:100) (Chemicon International Inc., Billerica, MA) diluted in 1% TBS-Tween and 0.5% low-fat milk. After rinsing three times with TBS-T 0.5% low-fat milk, membranes were incubated for 1 h at RT, with an alkaline phosphatase-linked secondary antibody antirabbit IgG 1:20 000 in 1% TBS-T and 0.5% low-fat milk (GE Healthcare, Buckinghamshire, UK). For endogenous control immunolabeling, primary antibody solution consisted of mouse monoclonal anti-GAPDH (1:10 000) (Millipore, MA). Protein immunoreactive bands were visualized in a Versa-Doc Imaging System (model 3000, BioRad Laboratories, CA), following incubation of the membrane with ECF reagent (GE Healthcare, Buckinghamshire, UK) for 5 min. Densitometric analyses were performed by using the ImageQuant software.

Immunocytochemistry. Cells were fixed with 4% paraformaldehyde (PFA). After washing three times with PBS, unspecific binding was prevented by incubating cells in a 3% BSA and 0.3% Triton X-100 solution for 30 min at RT. Cells were kept overnight at 4 °C in a primary antibody solution, then washed with PBS the following day, and incubated for 1 h at RT with the corresponding secondary antibody. Antibodies were used as listed: mouse monoclonal anti-Tuj1 (Covance, Princeton, NJ) (1:100), mouse monoclonal anti-NeuN (Millipore) (1:100), rabbit polyclonal anti-GFAP (1:100) (Cell Signaling Tech., Beverly, MA) prepared in 0.1% Triton X-100, 0.3% BSA solution; Alexa Fluor 594 goat antimouse; Alexa Fluor 488 goat antirabbit (both at 1:200 in PBS, from Invitrogen). For nuclear labeling, cell preparations were stained with Hoechst-33342 (2 μg/mL) (Invitrogen) in PBS 5 min at RT and mounted in Dakocytomation fluorescent medium (Dakocytomation Inc., Carpinteria, CA). Fluorescent images were acquired using a confocal microscope (LSM 510 Meta, Carl Zeiss).

In order to visualize the NPs' internalization, cells were incubated overnight with the RA-releasing NPs (10 μg/mL) and then fixed in methanol/acetone 1:1 for 20 min at −20 °C. After fixation, nonspecific binding sites were blocked with 6% BSA (Sigma) in PBS for 1 h. Cells were subsequently incubated with the primary antibody mouse monoclonal anti-FITC (1:100, Sigma) in PBS containing 0.3% BSA (Sigma). Thereafter, coverslips were rinsed in PBS and incubated for 1 h at RT, with the secondary goat antimouse Alexa 594 (1:200, Invitrogen). After rinsing with PBS, cell preparations were incubated with Hoechst-33342 (2 μg/mL, Invitrogen) in PBS for 5 min at RT. Finally, the preparations were mounted using Dako fluorescent mounting medium (Dakocytomation). Fluorescent images were acquired using a confocal microscope (LSM 510 Meta, Carl Zeiss).

TUNEL Assay. SVZ cultures were fixed with 4% PFA for 30 min, at RT, rinsed in PBS and permeabilized in 0.25% Triton X-100 (Sigma) for 30 min at RT. Thereafter, coverslips were incubated for 20 min in 3% H_2O_2 and reacted for terminal transferase (0.25 U/μL) biotinylated dUTP (6 μM) nick-end labeling of fragmented DNA in TdT buffer (pH 7.5) (all from Roche, Basel, Switzerland) for 1 h 30 min at 37 °C in a humidified chamber. The enzymatic reaction was stopped by 15 min incubation in 300 mM NaCl and 30 mM sodium citrate (both from Sigma) buffer. Following an additional rinse in PBS, cultures were incubated for 30 min at RT

with the avidin−biotin−peroxidase complex (1:100; Vector Laboratories Inc., Burlingame, CA). Peroxidase activity was revealed by the DAB chromogen (0.025%; Sigma) intensified with 0.08% $NiCl_2$ in 30 mM Tris-HCl (pH 7.6) buffer containing 0.003% H_2O_2. The cell preparations were then dehydrated in an ethanol gradient (70%, 2 min; 80%, 2 min; 90%, 2 min; 95%, 2 min; 100%, 2 min), cleared in xylene (3 min), and mounted using DEPEX mounting medium (Fluka Chemie AG, Buchs, Switzerland). Photomicrographs of TUNEL labeling were recorded using a digital camera (Axiocam HRC, Carl Zeiss) adapted to an Axioskop 2 Plus fluorescent microscope (Carl Zeiss).

PI Incorporation. Propidium iodide (3 μg/mL, Sigma) was added 40 min before the end of the 48 h of incubation with RA^+-NPs. Thereafter, cells were fixed with 4% PAF for 30 min, rinsed in PBS, stained with Hoechst-33342 (2 μg/mL; Invitrogen) in PBS for 5 min at RT, and mounted in Dakocytomation fluorescent medium (Dakocytomation Inc.). Photomicrographs of PI uptake labeling were recorded using a digital camera (Axiocam HRC, Carl Zeiss) adapted to an Axioskop 2 Plus fluorescent microscope (Carl Zeiss).

BrdU Incorporation. SVZ cell cultures were treated for 48 h with NP^+-RA with concentrations ranging from 1 ng/mL to 10 μg/mL for differentiation conditions and 100 ng/mL to 10 μg/mL for proliferative conditions. BrdU (10 μM; Sigma) was added in the last 4 h of each NP^+-RA treatment. For the differentiation conditions, cells were seeded in glass coverslips (as described previously). However, for the proliferative conditions, this assay was performed on primary neurospheres that at the end of 48 h treatment were collected from the Petri dishes into eppendorfs and adhered to superfrost microscope slides (Thermo Scientific, Braunschweig, Germany) by cytospin centrifugation (1200 rpm, 5 min; Cellspin I, Tharmac GmbH, Waldsolms, Germany). Afterward, the protocol was common for both conditions as follows. Cells were fixated in 4% PFA for 30 min and rinsed in 0.15 M PBS. BrdU was unmasked following successive passages in 1% Triton X-100 (Sigma) for 30 min, ice cold 0.1 M HCl for 20 min, and 2 M HCl for 40 min at 37 °C. Cells were neutralized with sodium borate buffer (0.1 M $Na_2B_4O_7 \cdot 10H_2O$, pH 8.5; Sigma) for 15 min at RT, rinsed in PBS, and then incubated in a blocking solution with 3% bovine serum albumin (BSA; Sigma) and 0.3% Triton X-100 in PBS for 30 min at room temperature. SVZ cultures were incubated with mouse anti-BrdU conjugated with Alexa Fluor 594 (1:100; Invitrogen) in PBS containing 0.3% Triton X-100 and 0.3% BSA overnight at 4 °C. Cell nuclei were counterstained with 6 μg/mL Hoechst-33342 in PBS for 5 min at RT and mounted in Dakocytomation fluorescent medium (Dakocytomation Inc.). Photomicrographs of BrdU-stained cells were recorded using a digital camera (Axiocam HRC, Carl Zeiss) adapted to an Axioskop 2 Plus fluorescent microscope (Carl Zeiss). The number of proliferating cells (BrdU-positive) were counted and expressed as percentage of total cells stained with Hoechst-33342 (Supporting Information Figure 3).

Statistical Analysis. Data are expressed as means ± standard error of mean (SEM). Statistical significance was determined by using Student's *t* test or one-way ANOVA followed by Dunnett's *post hoc* test for comparison with control or Neuman-Keuls for multiple comparison test, with $P < 0.05$ considered to represent statistical significance. All measurements were performed in the monolayer of cells surrounding the seeded SVZ neurospheres. For SCCI experiments, the percentage of neuronal responding cells (Hist/KCl ratio <0.8) was calculated on the basis of one microscopic field per coverslip, containing about 100 cells (40× magnification). Percentages of NeuN-, TUNEL-, or PI-positive cells were calculated from cell counts in five independent microscopic fields in each coverslip with a 40× objective (approximately 200 cells per field). Because no significant differences were found between experiments from different SVZ cell cultures, the corresponding data were pooled.

Acknowledgment. We thank the financial support of Marie Curie Grant (L.F.), MIT-Portugal Program (focus in Bioengineering, L.F.), Fundação para a Ciência e a Tecnologia (PTDC/CTM/099659/2008, L.F.; PTDC/SAU-NEU/68465/2006, J.O.M.; PTDC/SAU-NEU/104415/2008, L.B.), Instituto de Investigação Interdisciplinar (III/BIO/20/2005, J.M.), and Fundação Calouste Gulbenkian (FCG 96542, L.B. and F.A.).

Supporting Information Available: Supplementary figures and a movie. This material is available free of charge *via* the Internet at http://pubs.acs.org.

REFERENCES AND NOTES

1. Ferreira, L.; Karp, J. M.; Nobre, L.; Langer, R. New Opportunities: The Use of Nanotechnologies To Manipulate and Track Stem Cells. *Cell Stem Cell* **2008**, *3*, 136–146.
2. Hwang, N. S.; Varghese, S.; Elisseeff, J. Controlled Differentiation of Stem Cells. *Adv. Drug Delivery Rev.* **2008**, *60*, 199–214.
3. Ferreira, L.; Squier, T.; Park, H.; Choe, H.; Kohane, D.; Langer, R. Human Embryoid Bodies Containing Nano- and Microparticulate Delivery Vehicles. *Adv. Mater.* **2008**, *20*, 2285–2295.
4. Ferreira, L. S.; Gerecht, S.; Fuller, J.; Shieh, H. F.; Vunjak-Novakovic, G.; Langer, R. Bioactive Hydrogel Scaffolds for Controllable Vascular Differentiation of Human Embryonic Stem Cells. *Biomaterials* **2007**, *28*, 2706–2717.
5. Duester, G. Retinoic Acid Synthesis and Signaling During Early Organogenesis. *Cell* **2008**, *134*, 921–931.
6. Sachlos, E.; Auguste, D. T. Embryoid Body Morphology Influences Diffusive Transport of Inductive Biochemicals: A Strategy for Stem Cell Differentiation. *Biomaterials* **2008**, *29*, 4471–4480.
7. Kim, M.; Habiba, A.; Doherty, J. M.; Mills, J. C.; Mercer, R. W.; Huettner, J. E. Regulation of Mouse Embryonic Stem Cell Neural Differentiation by Retinoic Acid. *Dev. Biol.* **2009**, *328*, 456–471.
8. Szuts, E. Z.; Harosi, F. I. Solubility of Retinoids in Water. *Arch. Biochem. Biophys.* **1991**, *287*, 297–304.
9. Thunemann, A. F.; Beyermann, J. Polyethylenimine Complexes with Retinoic Acid: Structure, Release Profiles, and Nanoparticles. *Macromolecules* **2000**, *33*, 6878–6885.
10. Thunemann, A. F.; Beyermann, J.; Kukula, H. Poly(ethylene oxide)-*b*-poly(L-lysine) Complexes with Retinoic Acid. *Macromolecules* **2000**, *33*, 5906–5911.
11. Castro, G. A.; Orefice, R. L.; Vilela, J. M. C.; Andrade, M. S.; Ferreira, L. A. M. Development of a New Solid Lipid Nanoparticle Formulation Containing Retinoic Acid for Topical Treatment of Acne. *J. Microencapsulation* **2007**, *24*, 395–407.
12. Vasir, J. K.; Labhasetwar, V. Biodegradable Nanoparticles for Cytosolic Delivery of Therapeutics. *Adv. Drug Delivery Rev.* **2007**, *59*, 718–728.
13. Breunig, M.; Bauer, S.; Goepferich, A. Polymers and Nanoparticles: Intelligent Tools for Intracellular Targeting. *Eur. J. Pharm. Biopharm.* **2008**, *68*, 112–128.
14. Boussif, O.; Lezoualc'h, F.; Zanta, M. A.; Mergny, M. D.; Scherman, D.; Demeneix, B.; Behr, J. P. A Versatile Vector for Gene and Oligonucleotide Transfer into Cells in Culture and *In Vivo*: Polyethylenimine. *Proc. Natl. Acad. Sci. U.S.A.* **1995**, *92*, 7297–7301.
15. Akinc, A.; Thomas, M.; Klibanov, A. M.; Langer, R. Exploring Polyethylenimine-Mediated DNA Transfection and the Proton Sponge Hypothesis. *J. Gene Med.* **2005**, *7*, 657–663.
16. Tiyaboonchai, W.; Woiszwillo, J.; Middaugh, C. Formulation and Characterization of Amphotericin B-Polyethylenimine-Dextran Sulfate Nanoparticles. *J. Pharm. Sci.* **2001**, *90*, 902–914.
17. Kramer, M.; Stumbe, J. F.; Turk, H.; Krause, S.; Komp, A.; Delineau, L.; Prokhorova, S.; Kautz, H.; Haag, R. pH-Responsive Molecular Nanocarriers Based on Dendritic Core−Shell Architectures. *Angew. Chem., Int. Ed.* **2002**, *41*, 4252–4256.
18. Kim, D.; Choi, C.; Jeong, Y.; Jang, M.; Nah, J.; Kang, S.; Bang, M. All-Trans Retinoic Acid-Associated Low Molecular Weight Water-Soluble Chitosan Nanoparticles Based on Ion Complex. *Macromol. Res.* **2006**, *14*, 66–72.
19. Choi, Y.; Kim, S.; Kim, S.; Lee, K.; Kim, C.; Byun, Y. Long-Term Delivery of All-Trans-Retinoic Acid Using

Biodegradable PLLA/PEG-PLLA Blended Microspheres. *Int. J. Pharm.* **2001**, *215*, 67–81.
20. Lois, C.; Alvarez-Buylla, A. Proliferating Subventricular Zone Cells in the Adult Mammalian Forebrain Can Differentiate into Neurons and Glia. *Proc. Natl. Acad. Sci. U.S.A.* **1993**, *90*, 2074–2077.
21. Zhao, C.; Deng, W.; Gage, F. H. Mechanisms and Functional Implications of Adult Neurogenesis. *Cell* **2008**, *132*, 645–660.
22. Lledo, P. M.; Alonso, M.; Grubb, M. S. Adult Neurogenesis and Functional Plasticity in Neuronal Circuits. *Nat. Rev. Neurosci.* **2006**, *7*, 179–193.
23. Abdallah, B.; Hassan, A.; Benoist, C.; Goula, D.; Behr, J. P.; Demeneix, B. A. A Powerful Nonviral Vector for *In Vivo* Gene Transfer into the Adult Mammalian Brain: Polyethylenimine. *Hum. Gene Ther.* **1996**, *7*, 1947–1954.
24. Goula, D.; Remy, J. S.; Erbacher, P.; Wasowicz, M.; Levi, G.; Abdallah, B.; Demeneix, B. A. Size, Diffusibility and Transfection Performance of Linear PEI/DNA Complexes in the Mouse Central Nervous System. *Gene Ther.* **1998**, *5*, 712–717.
25. Lemkine, G. F.; Mantero, S.; Migne, C.; Raji, A.; Goula, D.; Normandie, P.; Levi, G.; Demeneix, B. A. Preferential Transfection of Adult Mouse Neural Stem Cells and Their Immediate Progeny *In Vivo* with Polyethylenimine. *Mol. Cell. Neurosci.* **2002**, *19*, 165–174.
26. Reynolds, B. A.; Weiss, S. Generation of Neurons and Astrocytes from Isolated Cells of the Adult Mammalian Central Nervous System. *Science* **1992**, *255*, 1707–1710.
27. Levison, S. W.; Goldman, J. E. Multipotential and Lineage Restricted Precursors Coexist in the Mammalian Perinatal Subventricular Zone. *J. Neurosci. Res.* **1997**, *48*, 83–94.
28. Gage, F. H. Mammalian Neural Stem Cells. *Science* **2000**, *287*, 1433–1438.
29. Agasse, F.; Bernardino, L.; Silva, B.; Ferreira, R.; Grade, S.; Malva, J. O. Response to Histamine Allows the Functional Identification of Neuronal Progenitors, Neurons, Astrocytes, and Immature Cells in Subventricular Zone Cell Cultures. *Rejuvenation Res.* **2008**, *11*, 187–200.
30. Goetz, A. K.; Scheffler, B.; Chen, H. X.; Wang, S.; Suslov, O.; Xiang, H.; Brustle, O.; Roper, S. N.; Steindler, D. A. Temporally Restricted Substrate Interactions Direct Fate and Specification of Neural Precursors Derived from Embryonic Stem Cells. *Proc. Natl. Acad. Sci. U.S.A.* **2006**, *103*, 11063–11068.
31. Agasse, F.; Bernardino, L.; Kristiansen, H.; Christiansen, S. H.; Ferreira, R.; Silva, B.; Grade, S.; Woldbye, D. P.; Malva, J. O. Neuropeptide Y Promotes Neurogenesis in Murine Subventricular Zone. *Stem Cells* **2008**, *26*, 1636–1645.
32. Kim, K. K.; Adelstein, R. S.; Kawamoto, S. Identification of Neuronal Nuclei (NeuN) as Fox-3, a New Member of the Fox-1 Gene Family of Splicing Factors. *J. Biol. Chem.* **2009**, *284*, 31052–31061.
33. Wohl, C. A.; Weiss, S. Retinoic Acid Enhances Neuronal Proliferation and Astroglial Differentiation in Cultures of CNS Stem Cell-Derived Precursors. *J. Neurobiol.* **1998**, *37*, 281–290.
34. Takahashi, J.; Palmer, T. D.; Gage, F. H. Retinoic Acid and Neurotrophins Collaborate To Regulate Neurogenesis in Adult-Derived Neural Stem Cell Cultures. *J. Neurobiol.* **1999**, *38*, 65–81.
35. Wang, T. W.; Zhang, H.; Parent, J. M. Retinoic Acid Regulates Postnatal Neurogenesis in the Murine Subventricular Zone-Olfactory Bulb Pathway. *Development* **2005**, *132*, 2721–2732.
36. Maden, M. Retinoic Acid in the Development, Regeneration and Maintenance of the Nervous System. *Nat. Rev. Neurosci.* **2007**, *8*, 755–765.
37. Lu, J.; Tan, L.; Li, P.; Gao, H.; Fang, B.; Ye, S.; Geng, Z.; Zheng, P.; Song, H. All-Trans Retinoic Acid Promotes Neural Lineage Entry by Pluripotent Embryonic Stem Cells *via* Multiple Pathways. *BMC Cell Biol.* **2009**, *10*, 57.
38. Etchamendy, N.; Enderlin, V.; Marighetto, A.; Vouimba, R. M.; Pallet, V.; Jaffard, R.; Higueret, P. Alleviation of a Selective Age-Related Relational Memory Deficit in Mice by Pharmacologically Induced Normalization of Brain Retinoid Signaling. *J. Neurosci.* **2001**, *21*, 6423–6429.
39. Crandall, J.; Sakai, Y.; Zhang, J.; Koul, O.; Mineur, Y.; Crusio, W. E.; McCaffery, P. 13-*cis*-Retinoic Acid Suppresses Hippocampal Cell Division and Hippocampal-Dependent Learning in Mice. *Proc. Natl. Acad. Sci. U.S.A.* **2004**, *101*, 5111–5116.
40. Fiorio Pla, A.; Maric, D.; Brazer, S. C.; Giacobini, P.; Liu, X.; Chang, Y. H.; Ambudkar, I. S.; Barker, J. L. Canonical Transient Receptor Potential 1 Plays a Role in Basic Fibroblast Growth Factor (bFGF)/FGF Receptor-1-Induced Ca^{2+} Entry and Embryonic Rat Neural Stem Cell Proliferation. *J. Neurosci.* **2005**, *25*, 2687–2701.
41. Platel, J. C.; Dave, K. A.; Gordon, V.; Lacar, B.; Rubio, M. E.; Bordey, A. NMDA Receptors Activated by Subventricular Zone Astrocytic Glutamate Are Critical for Neuroblast Survival Prior to Entering a Synaptic Network. *Neuron* , *65*, 859–872.
42. Danielyan, L.; Schafer, R.; von Ameln-Mayerhofer, A.; Buadze, M.; Geisler, J.; Klopfer, T.; Burkhardt, U.; Proksch, B.; Verleysdonk, S.; Ayturan, M.; *et al.* 2nd Intranasal Delivery of Cells to the Brain. *Eur. J. Cell Biol.* **2009**, *88*, 315–324.
43. Roy, I.; Stachowiak, M. K.; Bergey, E. J. Nonviral Gene Transfection Nanoparticles: Function and Applications in the Brain. *Nanomedicine* **2008**, *4*, 89–97.
44. Agasse, F.; Roger, M.; Coronas, V. Neurogenic and Intact or Apoptotic Non-neurogenic Areas of Adult Brain Release Diffusible Molecules That Differentially Modulate the Development of Subventricular Zone Cell Cultures. *Eur. J. Neurosci.* **2004**, *19*, 1459–1468.
45. Pinheiro, P. S.; Rodrigues, R. J.; Rebola, N.; Xapelli, S.; Oliveira, C. R.; Malva, J. O. Presynaptic Kainate Receptors Are Localized Close to Release Sites in Rat Hippocampal Synapses. *Neurochem. Int.* **2005**, *47*, 309–316.